remote sensing

MDPI

Article

Spatiotemporal Information Mining for Emergency Response of Urban Flood Based on Social Media and Remote Sensing Data

Hui Zhang [1], Hao Jia [1], Wenkai Liu [1], Junhao Wang [1], Dehe Xu [1], Shiming Li [1] and Xianlin Liu [1,2,*]

[1] College of Surveying and Geo-Informatics, North China University of Water Resources and Electric Power, Zhengzhou 450046, China; zhanghui2019@ncwu.edu.cn (H.Z.); 201601625@stu.ncwu.edu.cn (H.J.); liuwenkai@ncwu.edu.cn (W.L.); 201725203@stu.ncwu.edu.cn (J.W.); xdhwzs@126.com (D.X.); lishiming@ncwu.edu.cn (S.L.)
[2] Chinese Academy of Engineering, Beijing 100088, China
* Correspondence: liuxl@cae.cn

Abstract: The emergency response is crucial in preventing and mitigating urban floods. Both remote sensing and social media data offer distinct advantages in large-scale flood monitoring and near-real-time flood monitoring. However, current research lacks a thorough exploration of the application of social media data and remote sensing imagery in the urban flood emergency response. To address this issue, this paper, while extracting disaster information based on social media data, deeply mines the spatiotemporal distribution characteristics and dynamic spatial accessibility of rescue points. Furthermore, SAR imagery and social media data for monitoring urban flooding are compared. This study took the Zhengzhou 7.20 urban flood as a case study and created a methodological framework to quickly extract flood disaster information (flood, landslide, and rescue points) using these two types of data; spatiotemporal analysis and random forest classification were also conducted to mine valuable information. Temporally, the study revealed that disaster information did not increase proportionally with the amount of rainfall during the rainfall process. Spatially, specific regions with higher susceptibility to flooding, landslides, and rescue points were identified, such as the central region characterized by low drainage standards and high-density urban areas, as well as the eastern region with low-lying terrain. Moreover, this study examined the spatial accessibility of rescue resources in real flood scenarios and found that their service coverage varied throughout the day during and after the disaster. In addition, social media excelled in high-density urban areas' flood point extraction, while SAR performed better in monitoring floods at the edges of low-density urban areas and large water bodies, allowing them to complement each other, to a certain extent. The findings of this study provide scientific reference value for the optimal selection of rescue paths and the allocation of resources in the emergency response to urban floods caused by extreme rainstorms.

Keywords: flood disaster; social media data; remote sensing; spatiotemporal analysis; emergency response

check for updates

Citation: Zhang, H.; Jia, H.; Liu, W.; Wang, J.; Xu, D.; Li, S.; Liu, X. Spatiotemporal Information Mining for Emergency Response of Urban Flood Based on Social Media and Remote Sensing Data. *Remote Sens.* **2023**, *15*, 4301. https://doi.org/10.3390/rs15174301

Academic Editors: Pingping Luo, Van-Thanh-Van Nguyen, Binaya Kumar Mishra, Ahmed Elbeltagi, Reza Hassanzadeh and Baofu Li

Received: 13 July 2023
Revised: 25 August 2023
Accepted: 29 August 2023
Published: 31 August 2023

1. Introduction

Climate change and rapid urbanization continue to aggravate the problem of urban flooding. Climate change has led to frequent extreme rainstorms [1], and impervious surface expansion and inadequate drainage facilities in the process of rapid urbanization have exacerbated the occurrence of urban flooding [2,3]. Meanwhile, the concentration of people, property, and socioeconomic activities further exacerbates the adverse effects of flooding [4–6]. Many cities in China suffer from severe floods, especially in the rainy season [7], such as Beijing's rainstorms on 23 July 2021 and 16 July 2018; Wuhan's rainstorm in July 2016; and Zhengzhou's heavy rainfall and flood disaster events on 20 July 2021, which pose serious threats to people's lives and property safety. Urban flooding has become a serious problem that needs to be solved in many cities in China or worldwide, and has received widespread attention from government policy-making departments and stakeholders [8].

Generally, the short-term road inundation in urban areas caused by heavy rainfall is shallow, which will cause temporary blockage of road vehicles, and people's social activities will soon return to normal. However, long-term extreme rainstorms will lead to serious road congestion, and population travel safety will be seriously threatened [9]. Commonly used measures, such as the improvement of drainage capacity and low-impact development measures, have limited effects on relief from severe rainstorms and floods [8,10]. In this case, the emergency response can minimize the losses from flood disasters [11,12]. The spatial location of flood disasters and their dynamic analysis are crucial to the deployment and implementation of the emergency response for disaster managers [13].

Many studies have developed a series of methods and data sources to determine the spatial location and severity of flood disasters, such as hydrodynamic models [14] and remote sensing images [15,16]. However, in complex urban environments, extremely heavy rain is difficult to predict accurately and the mechanisms of urban floods are not yet clear; both lead to difficulty in accurately simulating and predicting floods through models [17]. Urban pluvial floods usually occur in a few hours, and the urban internal environment is full of high spatial heterogeneity, which makes it insufficient for the temporal and spatial resolution of remote sensing images to meet their needs [18,19]. Due to its capability to penetrate clouds and wide spatial coverage [20], radar remote sensing has been utilized for river flood monitoring. However, its application in urban flood monitoring is limited. Urban floods often occur within a few hours or a day or two, and urban areas have complex features. Solely relying on SAR imagery with its spatial–temporal resolution cannot meet the demands of urban flood monitoring. SAR imagery is less effective in extracting water bodies in densely populated and built-up areas, so the monitoring of flooding in cities requires the use of other means.

Social media data, such as Twitter, Facebook, Weibo, etc., provide new opportunities for the extraction of urban flooding information [21,22]. This type of dataset includes real-time disaster information with locations released by many geographic volunteers on social media platforms. Therefore, compared with hydrodynamic models and remote sensing images, it has better timeliness and informativeness. At present, there has been some research using social media data for flood disaster location extraction and related extension research. Some studies [23–27], on the basis of the text or picture information of social media data, have used machine learning classification algorithms to obtain flood inundation location and range information. Other studies have utilized social media data as supplementary data, combined with remote images [28,29] or urban hydrological modeling [30,31], to extract the flood range. In related extension research, Zhang et al. [32] identified flood locations by combining social media data and other data sources, divided the main urban area of Wuhan into eight types of urban functional areas, and constructed a flood location "urban portrait".

Social media data with location and time can reveal the spatial or temporal patterns of flood events for the flood emergency response [33,34]. Thus, existing studies have started to explore the dynamic changes in floods from temporal or spatial perspectives. Temporally, some studies have analyzed the relationship between rainfall and information dissemination or the public response with the help of social media data [35,36]. In fact, the relationship between specific disaster information and rainfall has more obvious guiding significance for emergency responses, and there is still a lack of exploration. Spatially, some conventional spatial analysis methods in GIS, such as kernel density and spatial autocorrelation analysis methods, have been used to explore the spatial concentration degree of flood points. Liu et al. [37] used kernel density estimation and spatial autocorrelation analysis to study the spatial distribution characteristics of flooding points during 2013–2017. Feng et al. [33] used hot spot analysis to detect clusters of rainfall and flooding-relevant tweets on a daily scale. Kankanamge et al. [34] used the inverse distance weighted (IDW) interpolation method to identify the distribution of disaster impact levels based on Tweets.

In addition, the space–time cube in GIS can integrate temporal and spatial information at the same time [38], providing effective and intuitive means to mine dynamic information in many fields, such as traffic accidents [39,40] and diseases [41]. However, at present, this method has rarely been used for flood disasters.

In addition, spatial accessibility analysis in GIS has been employed to analyze the service areas of major infrastructure, such as metros [42], schools [43], fire houses, and police stations [44], in floods. Masuya et al. [45] selected houses with specific standards as emergency shelters in floods and analyzed their spatial distribution and accessibility using GIS. Shi et al. [46,47] attempted to find the impact of river-flooding inundation levels on emergency response times in Shanghai tourist attractions under different rainfall and land use scenarios. These studies mainly relied on hydrodynamic models to simulate flood inundation under different storm intensities and did not fully harness the real flood disaster information extracted from social media data. Furthermore, emergency rescue resources are not limited to fixed fire stations and hospitals. The rescue points provided by social media in disaster events are also crucial. In general, the current research on mining flood disaster information from a spatiotemporal coupling perspective for the urban emergency response is still limited.

Based on the analysis above, current research lacks a thorough exploration of the application of social media data and remote sensing imagery in the urban flood emergency response. To address this issue, this paper, while extracting disaster locations based on social media data, deeply mines their spatiotemporal distribution characteristics and spatial accessibility of rescue points. Furthermore, SAR imagery and social media data for monitoring urban flooding are compared. This study utilized the Zhengzhou 7.20 rainstorm and flood disaster as a case study. It aimed to integrate near-real-time social media data and SAR images for extracting flood disaster information and conducting spatiotemporal analysis to mine valuable information to facilitate the implementation of emergency responses. First, we coupled a natural language processing platform, GIS, and social media data and POI data to build a methodological framework for the rapid extraction of real-time flood disaster information (flood, landslide, and rescue points). The effectiveness of social media data and SAR remote sensing imagery in urban flood monitoring was compared. Then, several spatiotemporal analysis methods, including kernel density, spatial autocorrelation, space–time cube, and network analysis, were employed to (1) analyze the response relationship between rainfall and the flood disaster; (2) mine the overall and spatiotemporal dynamic distributions of the flood disaster; (3) evaluate the space accessibility of the rescue sites; and (4) assess the effectiveness of SAR remote sensing imagery and social media data in urban flood monitoring.

2. Materials and Methods

2.1. Study Area

Zhengzhou is a national central city in China and the capital of Henan Province, located in the central northern part of the province (Figure 1). The selected region has a temperate continental climate with a mean annual precipitation of 625.9 mm. The study area selected for this paper is located in the main urban area of Zhengzhou City, and includes five districts: Huiji (HJ), Zhongyuan (ZY), Guancheng (GC), Jinshui (JS), and Erqi (EQ) Districts, with a total population of 5.016 million, accounting for 39.8% of the total population of Zhengzhou City and a study area of 1017 km^2.

During the period from 20 July to 22 July 2021, the accumulated rainfall in Zhengzhou reached 787 mm, which was more than the average annual rainfall in previous years. On 20 July, the maximum hourly rainfall reached 201.9 mm, surpassing the historical hourly maximum rainfall in mainland China. This typical urban rainstorm and flood catastrophe caused serious urban pluvial and fluvial floods, resulting in significant socioeconomic losses and casualties, which aroused widespread concern around the world. Many urban facilities (roads, buildings, and underground spaces) were flooded, roads collapsed, and power and communication lost their functions. By analyzing the processes of this event, the heavy rainfall first triggered the flood, then a secondary disaster road collapse occurred, and, finally, the emergency rescue response occurred. Thus, under the severe situation of increasing extreme rainfall, the information mining of the disaster processes of this event is helpful for emergency rescue and loss reduction of such events.

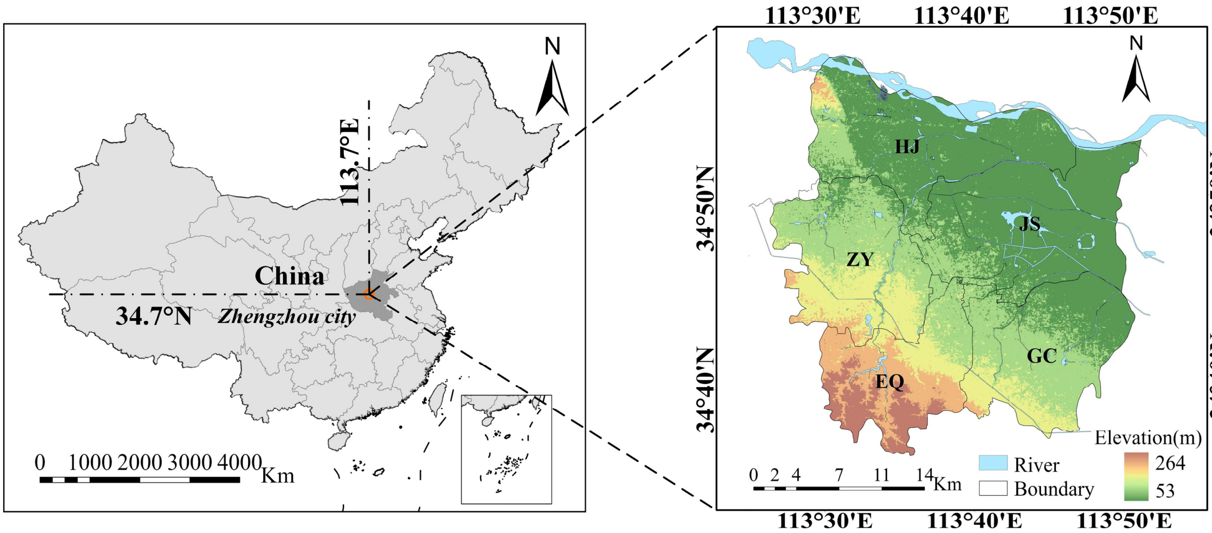

Figure 1. Geographic location and specifications of the study area.

2.2. Data Sources and Preprocessing

Weibo text data provided by the Chinese social media network platform Sina were used mainly for the extraction of disaster locations [48]. Considering the time span of the 7.20 extreme rainstorm in Zhengzhou, this study used Python web crawler technology to obtain a total of 22,860 texts from Zhengzhou City from 19 to 23 July 2021, taking "Zhengzhou rainstorm" as the keyword, with each Weibo record containing several fields, such as user ID, posting time, posting content, posting location, and posting tool.

In the context of the rapid development of multisource geographic information, POI data have been applied by various scholars in the study of road extraction due to their rich data volume, wide coverage, and accuracy of information [49,50]. POI road data were crawled from Amap (https://www.amap.com/, accessed on 1 November 2021), with a spatial scope of 2546 roads in the main city of Zhengzhou. In this paper, POI data were used to match Weibo text data to provide spatial location information for flood disasters.

This study collected GF-3 SAR images before (15 July 2021) and during (20 July 2021) the flood disaster in the study area. The preprocessing of SAR images primarily involved radiometric calibration, filtering and denoising, and geometric correction. Radiometric calibration converted the digital values of the SAR images into backscattering coefficients, which represented the radar reflectivity per unit area within the ground range, facilitating the comparison between SAR images acquired at different times. The SAR images were affected by significant speckle noise, which limited the accuracy of change detection in the SAR images [51]. Therefore, Frost filtering was used to suppress speckle noise in the GF-3 SAR images, ensuring the accuracy of the classification results. Geometric correction was performed on the images by manually selecting control points.

2.3. Methodology

A method framework (Figure 2) was created by integrating the NLPIR (Natural Language Processing and Information Retrieval Sharing Platform) with social media data, POI data, and GIS tools to extract real-time flood disaster information (flood, landslide and rescue).

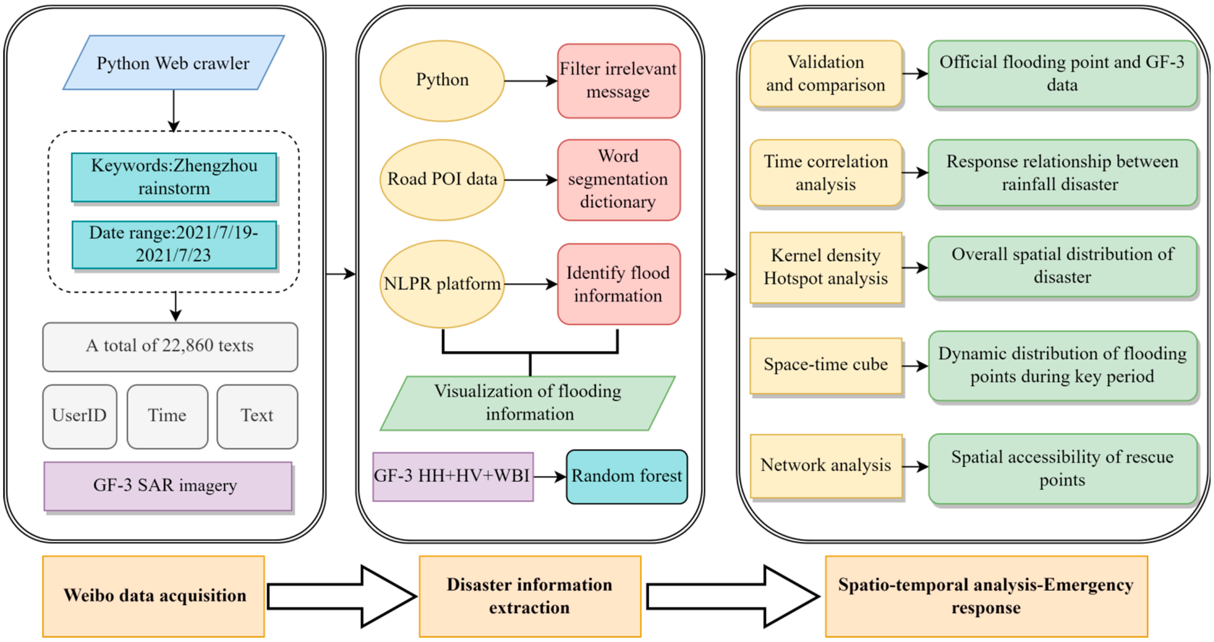

Figure 2. Methodological workflow of this study.

2.3.1. Rapid Extraction for Flood Disaster Information

Firstly, urban flooding hotspot text information was extracted using the Python tool. Secondly, the Python re module was used to filter out special characters that did not affect the meaning of the text. The Chinese deactivation word list was imported, and the Jieba module was used to deactivate the text and remove words with no real meaning. Thirdly, a user subword dictionary was created using Jieba based on the Zhengzhou POI data, totaling 2546 words. Then, the identification of different types of disaster information was built based on the NLPIR platform. The created POI user dictionary was imported into the NLPIR platform, and Weibo text data were processed for content segmentation, key word annotation, and lexical classification [52]. The main functions of NLPIR include Chinese segmentation, part-of-speech tagging, named entity recognition, and keyword extraction. The NLPIR platform, with the advantages of Chinese word separation processing, can quickly and accurately process large volumes of data in batches [38]. A total of 2546 names of different roads were filtered. Based on the keywords "Flooding", "Inflow", "Backflow", "Landslide" and "Rescue information", disaster information was successfully identified to determine the names of road sections where flooding and landslides occurred, as well as the locations of rescue points. Finally, geographic coordinates were obtained with the help of the Baidu Map Location tool and visualized in ArcGIS.

2.3.2. Spatiotemporal Analysis

Kernel Density and Spatial Autocorrelation

Kernel density is usually used to measure the degree of spatial clustering of point data, especially urban flood hotspot points. It applies a moving window and takes into account the spatial location of points in the window compared with ordinary density values. The kernel density method is a density distribution model for spatial features with distance decay effects that can be used to calculate the density of randomly distributed points in a neighborhood and output a raster image. A higher kernel density value indicates a more spatially concentrated distribution of disaster data, and the kernel density estimation Equation (1) is as follows [37]:

$$f_n(x) = \frac{1}{nh}\sum_{i=1}^{n} k\left(\frac{x - X_i}{h}\right) \quad (1)$$

where $k\left(\frac{x-X_i}{h}\right)$ is the kernel function, h is the bandwidth and represents the distance from valuation point x to point X_i, and n is the number of points in the window.

In this paper, the spatial autocorrelation method was used to analyze the spatial pattern of flooding, landslides, and rescue points. Unlike kernel density estimation, the spatial autocorrelation tool can measure the spatial autocorrelation of elements according to their positions and attribute values at the same time. The pattern of elements can be clustering, discrete, or random. In this paper, global Moran's I was first utilized to examine whether there was spatial autocorrelation in the whole study area. The calculation results of parameter I, the Z-test, and p value all showed that disaster information had a globally significant clustering effect. Then, the local spatial correlation (local Moran's I) was used to identify the spatial concentration pattern. The formula related to local space is as follows [37]:

$$I(i) = \frac{n(x_i - \overline{x})\Sigma_j W_{ij}(x_j - \overline{x})}{\Sigma_i (x_i - \overline{x})^2} \tag{2}$$

where x_i is the observation value of area i, and in this paper, it is the number of flooding, landslide, and rescue points in the grid; $\overline{x}$ is the average value; and W_{ij} is the spatial weight matrix, indicating the spatial weights of the grid cells i and j, where W_{ij} = 1 if grid cells i and j are adjacent, and W_{ij} = 0 otherwise.

Space–Time Cube and Emerging Hot Spot Analysis

In this study, the spatiotemporal cube tool was employed to investigate the spatiotemporal distribution characteristics, temporal evolution processes, and spatiotemporal hotspot analysis of flooding points [39]. Among the flood disasters in Zhengzhou City caused by the "7.20" torrential rainfall, 20 July witnessed the most severe flooding, with a significantly higher number of newly identified flood points compared with other disaster types, and distinct spatial features. Therefore, this research takes the flooding points from this particular day as an example and utilizes the spatiotemporal cube to illustrate their dynamic changes in time and space.

The spatiotemporal cube model was constructed by aggregating sample points into spatiotemporal columns (Figure 3), creating a spatiotemporal cube. This cube facilitates the visualization and analysis of spatiotemporal data through methods like time series analysis and integrated spatial and temporal pattern analysis [53]. In this study, flooding points within a 2 km radius every 6 h were considered as sample points. These sample points were then aggregated into a single cube, thus establishing a spatiotemporal cube model for flooding points. Consequently, by aggregating flood points at different spatiotemporal scales, the spatiotemporal variation characteristics and trends of flood points in Zhengzhou city on 20 July could be obtained and analyzed.

Spatial Accessibility

In cases of heavy urban rainfall and flooding, public safety and emergency response incidents require the prompt arrival of the emergency response department at the scene to address and assist people, with central urban areas typically necessitating an arrival time of 5 to 15 min [42]. GIS network analysis is a commonly employed method in assessing urban infrastructure accessibility. Previous studies have used this method to evaluate the spatial accessibility of facilities, such as medical and firefighting services, during flood events [43,47]. The advantage of this approach lies in its simultaneous consideration of travel time and distance costs.

In this study, when calculating the spatial accessibility of rescue points (also known as service coverage), two essential conditions need to be set: the obstruction to vehicle passage and vehicle speed. This study posits that road passages were hindered by flood and landslide points extracted from social media during this flood event. When the depth of flooding surpasses a vehicle's air intake height, safe vehicle passage becomes impossible, leading to road disruptions. Vehicle speeds are set at the highest speed limits of the roads.

Drawing from the study by the Chinese Urban Road Traffic Planning and Design Code (GB50220-95), the speed limits for roads of various categories are as follows [47]: 60 km/h for expressways, 40 km/h for primary roads, 30 km/h for secondary roads, 25 km/h for tertiary roads, and 15 km/h for local roads. Subsequently, utilizing the Service Area tool within ArcGIS Pro's network analysis, this study calculates and analyzes the service coverage and variations within 5 min, 10 min, and 15 min intervals for rescue points during different time periods of the disaster (20 July) and post-disaster (22 July).

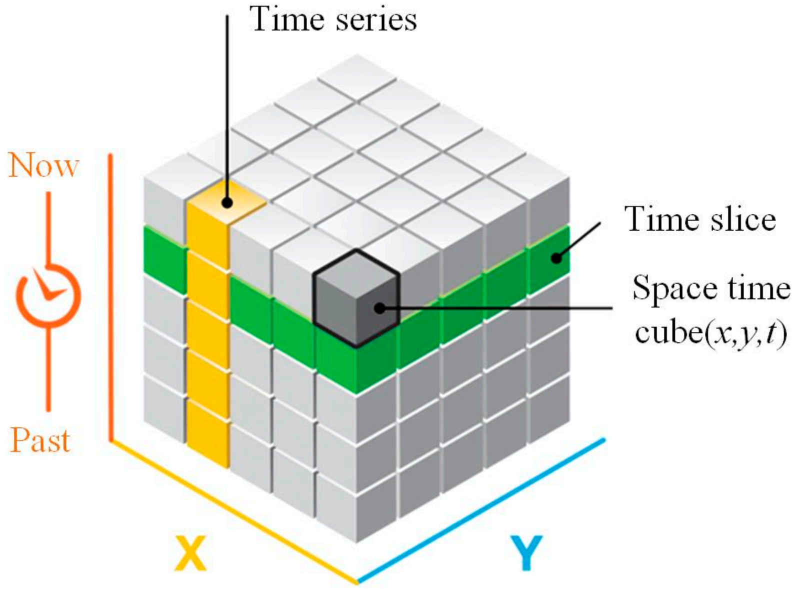

Figure 3. Space–time cube model diagram.

2.3.3. Random Forest Classification

Random forest classification is a widely adopted classifier known for its numerous advantages, including short processing time and high accuracy. It is an ensemble classifier that evolved from regression decision trees. By using decision trees as weak classifiers and leveraging the Bootstrap resampling method to extract diverse samples from the original dataset, the random forest algorithm progressively constructs decision trees through regression and combines them to form a random forest [54]. This versatile algorithm can predict thousands of variables and is currently the most extensively applied classification method in remote sensing image analysis. Referencing Jia et al. [55] and Tian et al. [56], who used Sentinel 1 SAR images to extract water bodies, the two polarization bands of the GF-3 SAR image, HH and HV were used to calculate the water body index (WBI). The calculation formula is as follows:

$$\text{WBI} = ln(10 \times HV \times HH) - 10 \quad (3)$$

When the WBI value is greater than 0, it indicates water. When it is less than 0, it indicates non-water. *HH* polarization refers to the SAR emitting microwave signals with a horizontal orientation and receiving echoes with the same horizontal orientation; *HV* polarization means that the SAR emits microwave signals with a horizontal orientation and receives echoes with a vertical orientation.

The synthesized image using the three GF-3 SAR HH, HV, and WBI bands was used for random forest classification to extract the flood inundation area. Visual interpretation was conducted on two GF-3 SAR images, with samples of water and non-water areas carefully selected. Subsequently, the image classification was performed using the random forest classifier in ENVI 5.6, completing the classification process.

3. Results

3.1. Validation and Comparison of Flooding Point Extraction

To verify the accuracy of the extraction of flooding points from Weibo texts, this paper compared the flooding points extracted by the NLPIR platform with those announced by the official sector (Zhengzhou Traffic Police). During 19–23 July 2021, a total of 171 flooding points were extracted based on Weibo data, which was quite close in total number to the 184 flooding points announced by the official sector. Social media or official information often describe the location of flooding as a specific road intersection or a particular road segment. Therefore, when visualizing flooding, it is common to represent it using point data. However, for the same flooded area, due to its spatial characteristics, there may be variations in the reference points used in textual descriptions. The different text representations of the same flooding point resulted in slight differences in the position of the visualization of the flooding point in the display (Figure 4a). Thus, the accuracy of flooding point extraction was assessed by setting 100 m and 300 m buffer zones. The points within the buffer zone were considered to be the same flooding points. Within the 100 m buffer, the probability of the same flooding points was 56.5%; however, within the 300 m buffer, this probability was as high as 85%. Therefore, in this study, the flood point results extracted based on Weibo data were reasonable.

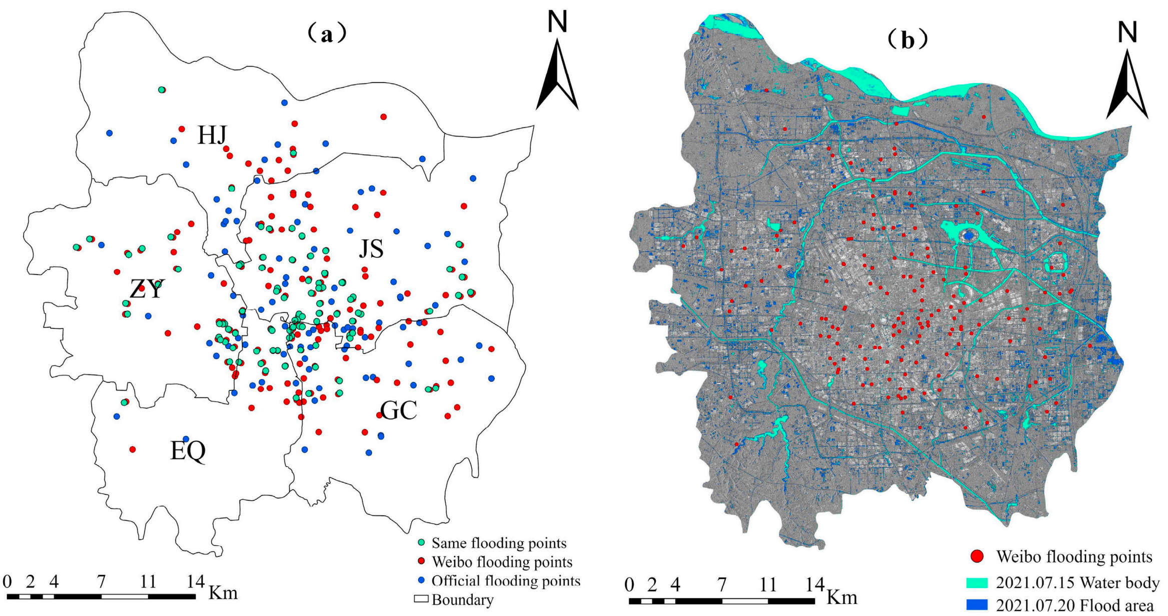

Figure 4. (**a**) Comparison map of Weibo flooding points and Zhengzhou traffic police official flooding points; (**b**) Flood inundation maps based on random forest algorithm and GF-3 imagery.

Based on GF-3 SAR imagery, the extent of flood inundation extracted is shown in Figure 4b. On 20 July, the flood inundation area was primarily distributed in the low-density built-up areas on the outskirts of the city and some large water bodies, such as the Jiangang Reservoir, the Yellow River section, and the eastern section of the Dongfeng Canal. However, the flooding points extracted from the Weibo platform and the official sector were mainly distributed in the high-density built-up areas in the central region of Zhengzhou. The flood detection based on GF-3 SAR imagery was less effective in high-density built-up areas. This was because the buildings and trees obstructed the road, causing the radar echo to fail to reflect the water bodies on the road. Compared with SAR data, social media data were a more effective source for extracting the extent of flooding in densely built urban areas.

3.2. Response Relationship between Rainfall and Floods

The response relationship between new disaster points and rainfall at different times is illustrated in Figure 5. Temporally, the study revealed that disaster information did not increase proportionally with the amount of rainfall during the rainfall process. In the initial stage of the storm between 12:00 on 19 and 09:00 on 20 July, the cumulative rainfall of 79.7 mm resulted in 72 new flooding points, being the highest of all periods, with 8 new landslide points and 12 new rescue points. In the middle stage of the rainstorm between 09:00 and 15:00 on 20 July, the cumulative rainfall was 103.8 mm, with 51 new floods, 8 new landslides, and 7 new rescue points, which was lower than that in the early stage. At the peak of the rainstorm between 15:00 and 21:00 on 20 July, the cumulative rainfall was 402 mm, but the number of new flooding points was a limited 29, much lower than those in the early and middle stages, with 10 new landslides and 6 new rescue points. During the decline in rainfall, it is worth noting that, although there was continuous rainfall from 22:00 on 20 July to 18:00 on 22 July, with a total rainfall of 143.3 mm, there were no new flooding points. Possible reasons for this were related to the gradual increase in flooding, which led to damage to communication and electrical facilities (some areas took the initiative to cut off the network and electricity to avoid harm to the crowd). During the final phase of the rainstorm, the total rainfall from 19:00 on 21 July to 00:00 on 23 July was 34.8 mm, with 19 new floods, 42 new landslides, and 41 new rescue points. The time scale of the rainfall showed that the early and mid-storm rainfall (183 mm) resulted in the creation of most of the flooding points. Landslides and rescue points were mainly concentrated in the late stage of rainfall.

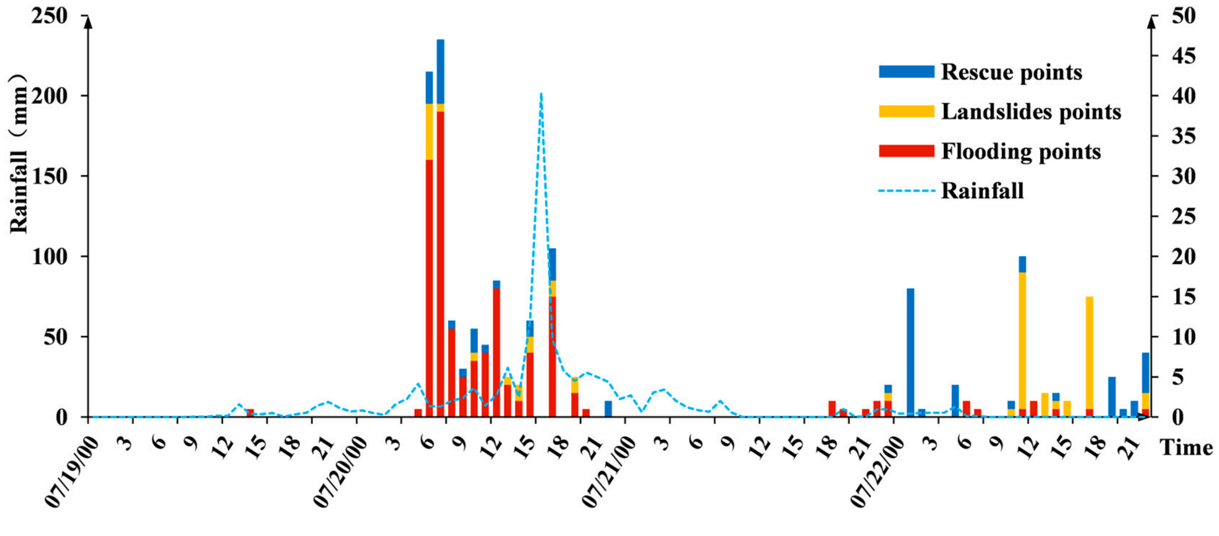

Figure 5. Relationship between rainstorm disaster information and hourly precipitation from 19 to 23 July.

3.3. Spatial Distribution of Flood Disaster Information

A disaster information statistical map based on administrative divisions is illustrated in Figure 6. During 7.20–7.22, a total of 169 flooding, 90 landslides, and 68 rescue points were extracted from the Weibo data in the main urban area of Zhengzhou. The JS district had the largest number of each kind of disaster point among all five districts, while the HJ district had the smallest number of each type of disaster point. Among the other three districts, the ZY and GC districts had the same number of flooding points, which was slightly higher than that in the EQ district. The number of landslide points and rescue points in the GC and EQ districts was approximate; however, their number of landslide points was lower than that in the ZY district, and the number of rescue points was slightly higher than that in the ZY district.

The kernel density indicated that the trend of the spatial concentration degree of flood, landslide, and rescue points was similar to a certain extent; that is, the concentration degree gradually decreased from the highest concentration area in the old town (near the boundary of the EQ, JS, GC, and ZY areas) to the surrounding areas (Figure 7a–c). Although their respective highest concentration regions were close in geographic location, the specific locations exhibited slight differences. For example, the highest-concentration region of the flood points was mainly situated in the border area between JS, EQ, and GC, while the landslide points were in ZY and the rescue points were in JS. Compared with the results of the kernel density analysis, the high–high clusters of flooding point hotspots with statistical significance were more concentrated within the old town. In addition, the flooding points had a larger coverage area than the landslides and rescue points. In contrast with the continuous distribution of rescue and flood points, the landslide points appeared to have a more obvious scattered clustering distribution.

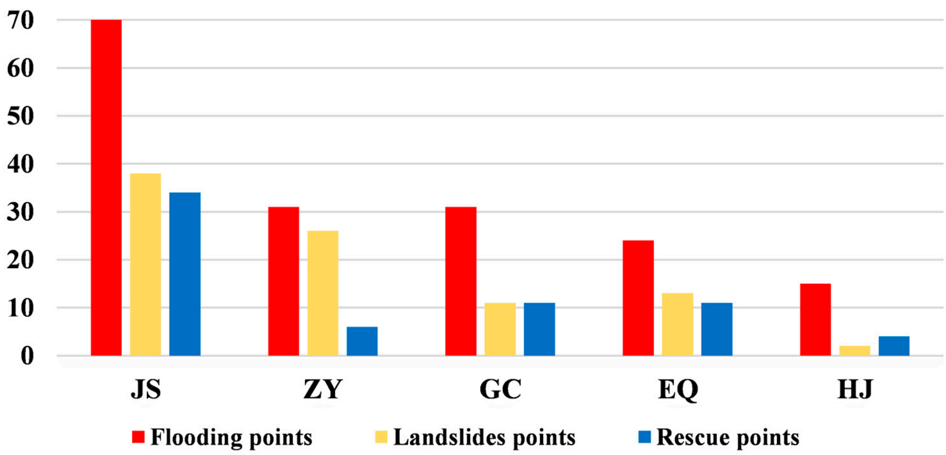

Figure 6. Statistical map of disaster information for Zhengzhou City.

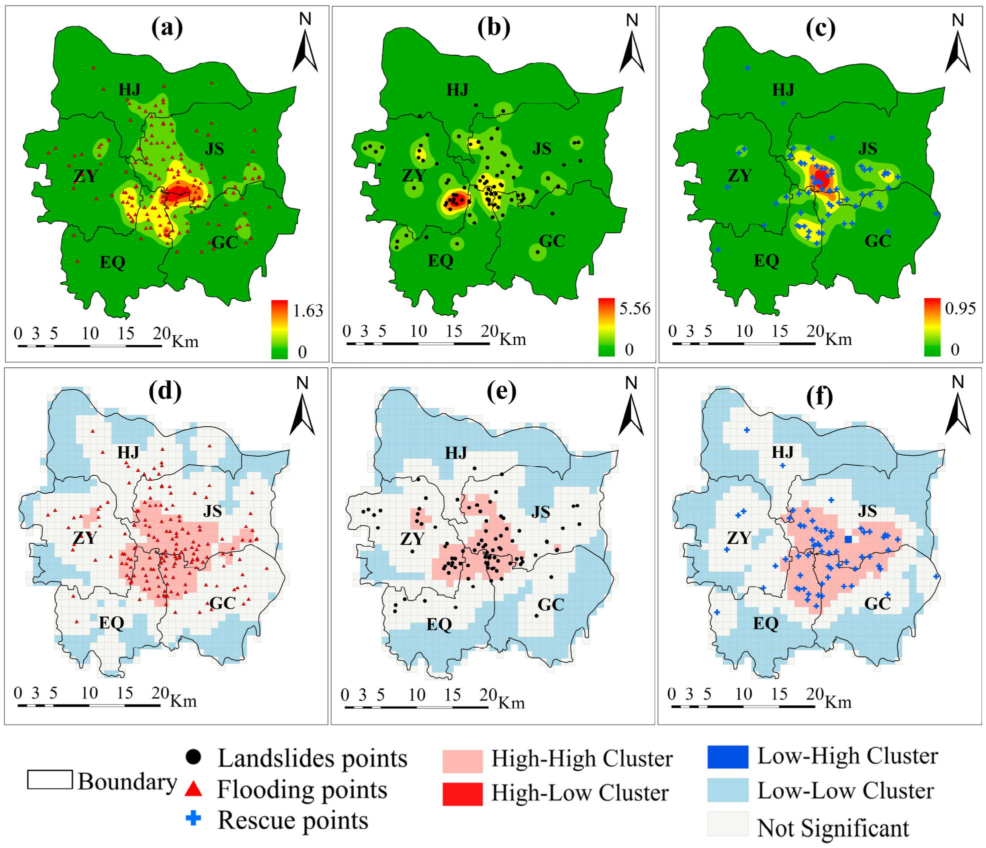

Figure 7. Kernel density (**a**–**c**) and clustering (**d**–**f**).

The results of local spatial autocorrelation analysis indicated that the main cluster patterns of flood, landslide, and rescue sites were high–high and low–low (Figure 7d–f). Among them, the high–high clustering pattern of the three kinds of disaster information points was mainly distributed in the central and eastern regions, while the low–low clustering pattern was mainly spread in the periphery of the study area, while the regions between the two patterns were the regions where the clustering was not significant.

3.4. Temporal and Spatial Dynamic Distribution of Flood Points

The three-dimensional visualization of the space–time cube model indicated that the spatiotemporal pattern of the new flood points was sporadically hot, mainly located in the western part of the JS district (Figure 8). This indicated that this region was an intermittent hot spot, and, at most, 90% of the time step intervals were statistically significant hot spots. The spatiotemporal pattern in other areas was not significant. There was only one new flooding point from 0:00–6:00 pm on 20 July; therefore, it is not shown here. Emerging hot spot analysis showed the spatial distribution of the hot spots of new flooding points in the three time periods from 6:00 to 24:00 on this day (Figure 9). As shown in Figure 9a, from 6:00 to 12:00 on 20 July, 94 new flooding points in this period were the highest in the four periods of the day, accounting for 62.3% of the total number of new flooding points throughout the day. Most flooding points were concentrated in the area surrounded by the South Third Ring Road, North Fourth Ring Road, West Third Ring Road, and Zhongzhou Avenue in the central high-density built-up area, and most of the region had an extremely significant (99% confidence) hot area. At the same time, there were small areas of extremely significant and significant (90% confidence) hot spots in the east and west, respectively. As shown in Figure 9b, during the 12:00–18:00 period, although the hourly rainfall reached an extreme value, the number of flood spots increased very little. Most of them were concentrated in the central and eastern regions, which were mainly related to the topography, with high values in the west and low values in the east. The most significant hot spots were concentrated in the southwestern part of the JS district in the central area, which was significantly smaller than that in the last period. However, due to the scattered flood points in the east, there was no significant distribution of hot spots. During the 18:00–24:00 period (Figure 9c), there were only 19 new flooding points, mainly situated in the central region. As the number of new flooding points in this period was small and spatially dispersed, there was no significant hot spot distribution.

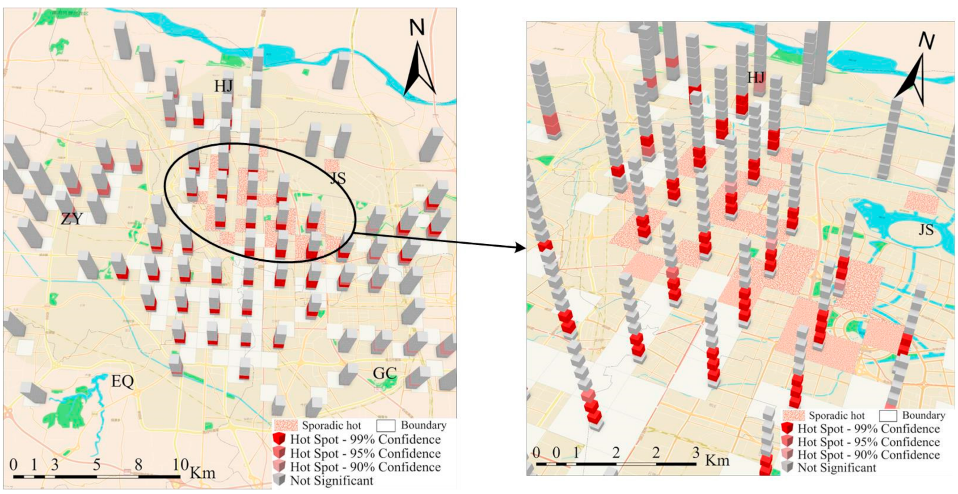

Figure 8. Space–time cube emerging heat map.

Emergency service areas were covered by 5, 10, and 15 min response times with three periods on 20 July and 22 July (Figures 10 and 11). Each day consisted of three time periods, namely the first time period, 06:00–12:00, the second time period, 12:00–18:00, and the third time period, 18:00–24:00. The results indicated that the service coverage of the rescue not only changed with time in a day, but also varied during and after the disaster.

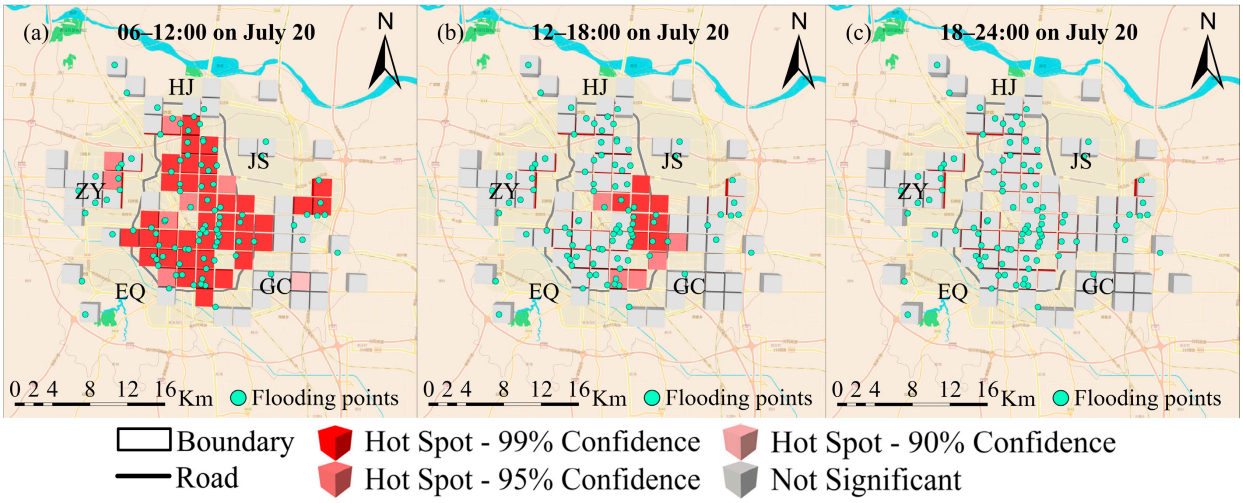

Figure 9. Emerging heat maps in different periods based on the space–time cube model: (**a**) 06–12:00 on July 20; (**b**) 12–18:00 on July 20; (**c**) 18–24:00 on July 20.3.5. Spatial Accessibility of Rescue Points.

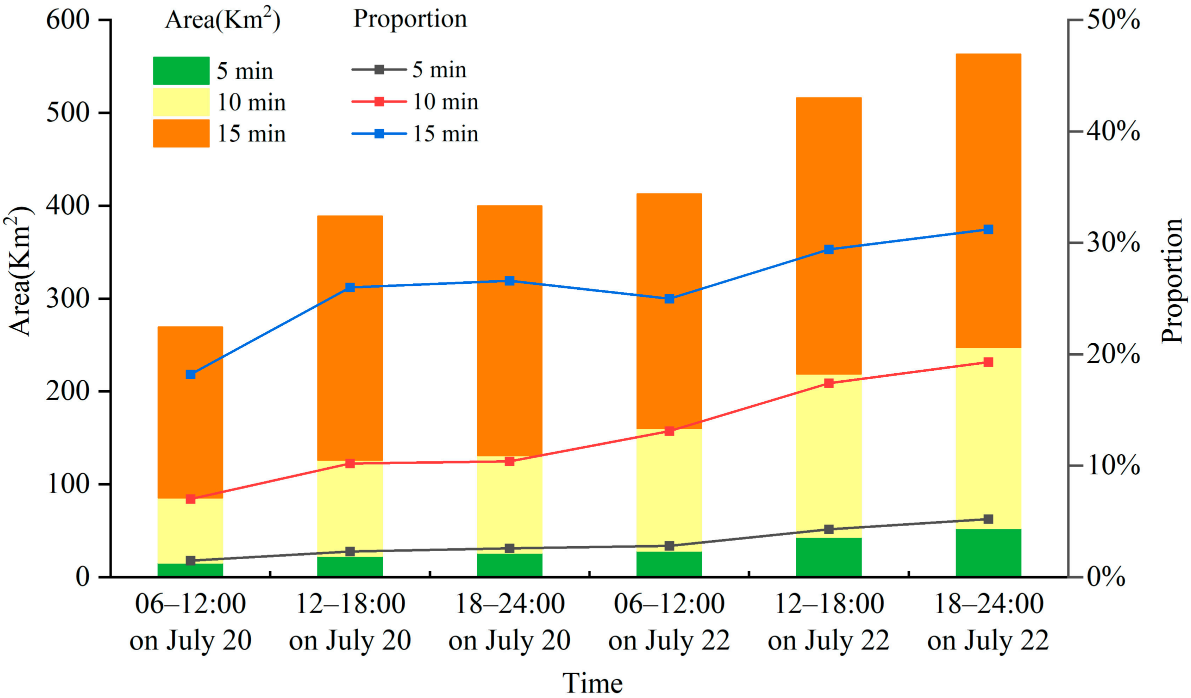

Figure 10. Emergency response service scope of rescue points in different periods.

On 20 July, emergency service generally improved slightly with time, most of which was distributed in the central and eastern parts of the study area, and a small part was located in the southwest. Within 5 min, the emergency service coverage was 1.5%, 2.3%, and 2.6%, respectively, from the first to the third period; within 10 min, the corresponding proportion became 7.0%, 10.2%, and 10.4%, respectively; and within 15 min, the corresponding proportion became 18.2%, 26.0%, and 26.6%, respectively. Obviously, for all response times, the corresponding area increased with increasing time. This was due to the spatial accessibility range of the rescue points increasing as the severity of the disaster escalated; however, this power was still insufficient. In addition, the emergency service area growth from the first to second period was significantly higher than that of the second to third period for all service response times. For example, when compared with the second period, the third period only had a 0.3% rise in the service area in 15 min. It could be observed that the increase in rescue capacity at night was very limited. Notably, some flooding points distributed in ZY were within the rescue scope until the third period; however, only a few areas located at the junction of JS and HJ were within the rescue range, as shown in the black ellipse in Figure 11. The growth trend of the service area on 22 July remained consistent with that on 22 July. However, the service area on 22 July effectively increased at the same service time and period in contrast with that on 20 July. Meanwhile, the spatial accessibility on 22 July demonstrated that the aggregation degree was more obvious in the central and eastern regions than that on 20 July. From another perspective, these situations confirmed that the central and eastern regions were the most severely affected regions of this flood. In addition to heavy rainfall, the main reason was that the terrain trend of the study area was high in the west and low in the east, and the urban built-up areas and population were dense, especially in the central region. Therefore, this region received the accumulation of rescue forces.

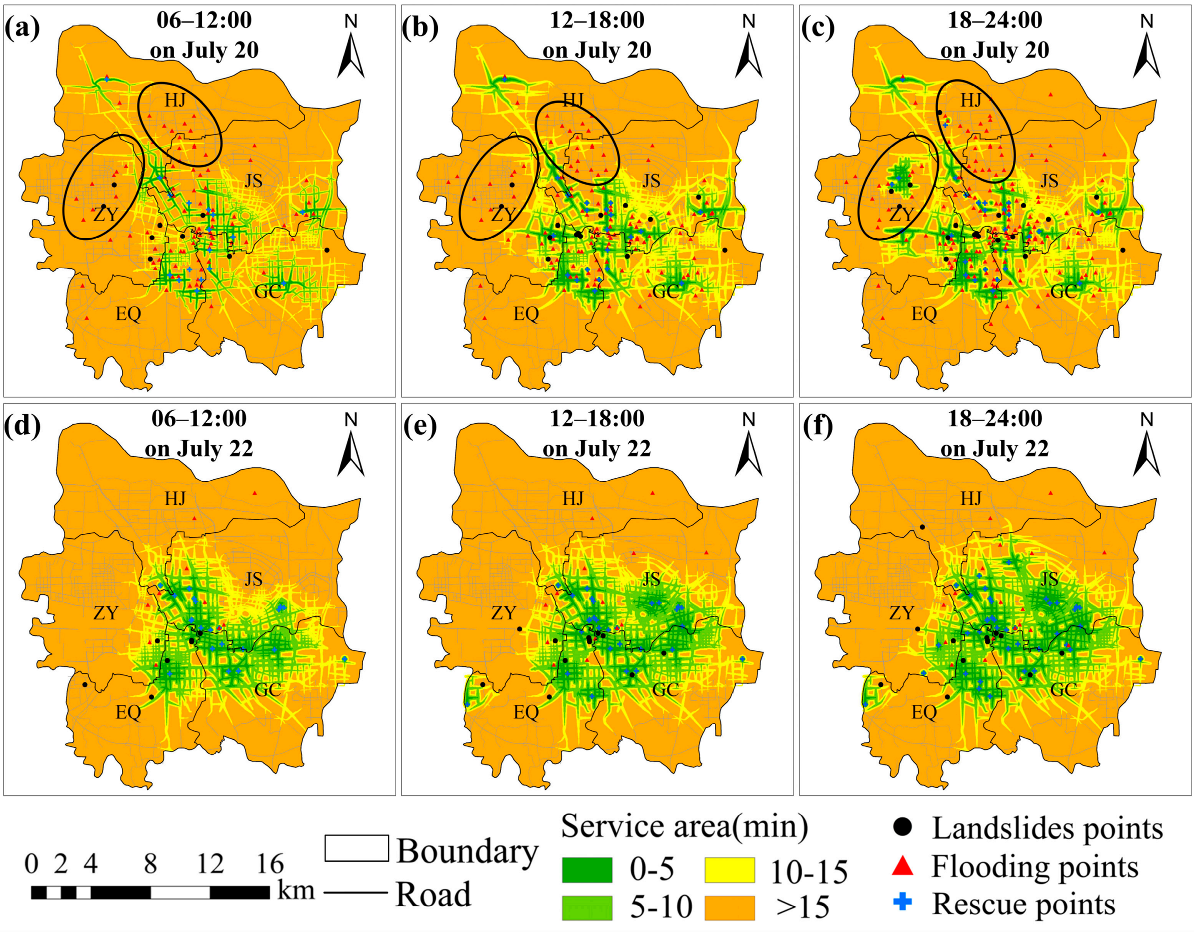

Figure 11. Spatial accessibility of rescue points in different periods: (**a**) 06–12:00 on July 20; (**b**) 12–18:00 on July 20; (**c**) 18–24:00 on July 20; (**d**) 06–12:00 on July 22; (**e**) 12–18:00 on July 22; (**f**) 18–24:00 on July 22.

4. Discussion

4.1. Comparison of Flood Point Extraction Based on Social Media and SAR Data

In densely populated areas, where buildings are concentrated, flooding events are more likely to capture public attention and media coverage. Social media data have a clear advantage in extracting flood points in these high-density built-up areas, because social media platforms often rely on information reported by geographically located volunteers [57].

These volunteers can promptly share text, photos, videos, and other information related to flooding, providing real-time reports on a disaster. However, GF-3 SAR performs better in monitoring floods in low-density built-up areas at the edges of cities and in large water bodies. GF-3 SAR can provide accurate flood monitoring in open areas [58]. In contrast, GF-3 SAR may face challenges in high-density urban areas, where buildings can obstruct its view, affecting the extraction of flood-related information, like road inundation. Therefore, social media data and GF-3 SAR have their respective advantages in flood monitoring in different environments and can complement each other. By combining these two data sources, a more comprehensive and accurate flood monitoring result can be achieved, which is of great significance for emergency response and disaster management.

4.2. The Potential Application of the Time–Response Relationship between Disaster and Rainfall in Early Warning

Analyzing the response relationship between direct triggering factors of flooding, rainfall, and disaster conditions can guide early warning. Previous studies considered the relationship between rainfall and social media activities or public response to be positive [17,36]. This paper further explored and identified the temporal correspondence between this rainfall and the number of new disasters, including flooding, landslide, and rescue points, and found that the quantity of disaster information did not increase with an increase in rainfall. For example, the number of newly added flooding points in the middle and later stages of rainfall was significantly lower than the number of newly added flooding points in the early stages of rainfall, indicating that the drainage facilities in the vast majority of flooding point occurrence areas were no longer able to cope with the early rainfall of this event. It is possible to identify the cumulative rainfall duration that will trigger the highest number of new flooding points. This can not only aid in further analyzing the relationship between urban floods and rainfall thresholds, but also evaluate the response capacity of the urban drainage system to rainstorms as a whole. Under extreme rainfall, the urban drainage network had lost its drainage capacity. In addition, this study also discovered an approximate 2–3 h lag between the peak rainfall volume and the peak number of new flooding points. This time lag was shorter than the approximately 3–4 h lag found by Fang et al. [17] between rainfall and social media activity. This suggests that severe flooding only occurs after a period of continuous heavy rainfall, leading to widespread attention on social media. Making full use of this time gap, timely issuance of rainstorm warning information, and the formulation of emergency plans have proven to be effective flood control methods.

4.3. Comparison of Spatiotemporal Distribution of Flood Disasters

Exploring the spatiotemporal distribution of disaster situations helps to distinguish areas highly affected by floods [34] and facilitates the initial configuration of emergency rescue resources. This study not only analyzed flooding points, like many previous studies, but also considered the spatial distribution of secondary disasters, such as landslides and rescue points, providing a more comprehensive understanding of the spatial aggregation patterns and their differences.

Flooding points were predominantly located in the old urban areas and the low-lying new urban areas. Their spatial characteristics were consistent with the distribution of floods in most cities in China [37,59]. This suggests that the old urban areas and low-lying new urban areas are key areas for flood emergency management. This is primarily determined by the urban spatial development model. The long construction history, low drainage pipe network standards, and densely populated buildings make the old urban areas prone to flooding. In urban expansion, flat or low-lying areas are preferred, which means that, even though the new urban areas have higher drainage pipe network standards, they are more susceptible to rainwater accumulation due to their terrain, especially during prolonged rainstorms. This flood event indicated that the rescue locations published on the social media platform were primarily concentrated in areas heavily affected by floods and densely populated.

Flood points had a larger coverage area compared with landslide and rescue points. While rescue and flood points exhibited continuous distribution, landslide points appeared to have a more scattered clustering distribution. Moreover, the high–high clustering regions of flood and rescue points were not only approximately equal in area, but also highly overlapped in space. The high–high clustering region of landslide points was mainly situated within the flood or rescue points range, but with a smaller area. This suggested that social emergency rescue primarily responded to floods, while the response to landslides was not as pronounced. The possible reason was that landslides mainly occur in the later stage of flooding, with a relatively small number and impact area. However, it should be noted that landslides occurring after rainfall and floods pose significant dangers to vehicles and pedestrians. Therefore, in emergency management, secondary disasters caused by floods should not be overlooked, and citizens should be promptly alerted to potential hazards.

4.4. The Application of Space Accessibility in Emergency Response

The dynamic spatiotemporal mining of flooding points and their spatial accessibility can provide targeted guidance for the allocation and scheduling of emergency resources in disasters. New flood points were concentrated in the central and eastern and western regions. Over time, new flood points continued to appear in the central and eastern regions, while the number of newly added flooding points in the western region gradually decreased. Therefore, emergency rescue supplies should be allocated to these three regions, with a particular focus on the central and eastern regions. Taking into account the variations in location and severity of flood sites, in this type of rainfall event, rescue resources from the eastern and western regions can supplement those in the central region.

The spatial access analysis of rescue points can evaluate the rescue capabilities and provide direct and effective guidance for disaster relief. In flood emergency rescue, flood and landslide points often pose obstacles, so a reasonable evaluation of the service scope of rescue points is crucial for evaluating the current rescue capacity. Yin et al. [43] and Shi et al. [47] mainly focused on the accessibility of fixed rescue points, such as fire stations and hospitals, in flood simulation scenarios and examined whether schools or tourist attractions of interest are located within their respective rescue service areas. However, emergency rescue resources are not limited to fire stations and hospitals; temporary shelters in disasters and locations that provide food for the affected population [60,61] are also part of the rescue effort. Furthermore, as demonstrated in this study, the rescue points may undergo changes. Compared with previous studies, this study focused on the dynamic emergency linkage of flood, landslide, and rescue points from a spatiotemporal perspective, aiming to supplement the accessibility analysis of rescue resources in real flood scenarios.

It was found that the spatial accessibility of rescue points differed not only across different time periods of the day, but also between the disaster and post-disaster phases. Whether on 20 July or 22 July, the accessibility service area of rescue gradually increased as the day progressed. On 20 July, the accessibility of rescue points in the central and eastern regions was significantly higher than in the western and northern regions. In the western region, the accessibility of rescue points did not increase until 18:00–24:00. However, the accessibility in the northern region remained low and showed minimal change. This difference may be attributed to the severity of flooding and its impact on the population. The densely populated and built-up areas in the central and eastern regions tend to attract more attention. With the weakening of the flood disaster, the spatial accessibility after the disaster significantly improved, particularly in the central and eastern regions, indicating an enhanced rescue capability. The post-disaster rescue efforts primarily focused on the central and eastern regions.

The limitations of this study are reflected in the fact that the data collection process did not account for variations in social media platforms and individual perceptions of flooding. Additionally, during the spatial accessibility analysis, due to the large study area, obtaining real-time traffic data was challenging, necessitating the use of traffic regulations to set vehicle speeds. In future research, improvements will be made to data acquisition.

5. Conclusions

In the process of the Zhengzhou 7.20 rainstorm flood disaster, a long period of heavy rainfall triggered floods, followed by secondary disasters of road landslides and emergency rescue responses. A methodological framework combining NLPIR, GIS, and social media was created to quickly extract near-real-time flood disaster information, including flood, landslide, and rescue points. Moreover, the study compared the differences in the effectiveness of SAR imagery and social media data for urban flood monitoring. Several spatiotemporal analysis methods were employed to explore the dynamic linkage of flood, landslide, and rescue points from a spatiotemporal perspective in the flood emergency response. The main conclusions were as follows:

(1) Temporally, the study revealed that disaster information did not increase proportionally with the amount of rainfall during the rainfall process. Instead, there was often a lag period of 2–3 h between the peak rainfall period and the small peak of new flooding points. Landslides and rescue points tended to be concentrated in the late stage of rainfall;
(2) Spatially, the research identified specific regions that exhibited higher susceptibility to flooding, landslides, and rescue points. These regions included the central region, characterized by low drainage standards and high-density urban areas, as well as the eastern region with low-lying terrain. This study also revealed the spatial and temporal dynamics of flood points, which shifted from the central region to the eastern region and eventually returned to the central region;
(3) This study examined the spatial accessibility of rescue resources in real flood scenarios and found that their service coverage varied throughout the day during and after the disaster;
(4) Social media data had advantages in extracting flood points in high-density urban areas, while SAR had advantages in monitoring floods in low-density urban areas at the city's edges and large water bodies. The two could complement each other, to a certain extent.

The findings of this study can provide a scientific foundation for the emergency response to urban floods triggered by extreme rainstorms, as well as subsequent disaster prevention and reduction efforts. However, it should also be noted that the flood information extracted based on social media data may be missing in the case of power communication interruption. In future research, actively combining big data from the urban Internet of Things or strengthening the repair of communication facilities will help to obtain more comprehensive disaster information for the flood emergency response.

Author Contributions: Conceptualization, H.Z.; methodology, H.J.; software, D.X.; validation, H.Z. and H.J.; formal analysis, J.W.; investigation, S.L.; resources, H.Z.; data curation, H.Z. and H.J.; writing—original draft preparation, H.Z. and H.J.; writing—review and editing, H.Z. and D.X.; visualization, H.J. and D.X.; supervision, X.L. and J.W.; project administration, W.L.; funding acquisition, H.Z. and D.X. All authors have read and agreed to the published version of the manuscript.

Funding: This research was funded by the National Natural Science Foundation of China (No. 42007423) and Henan Provincial Science and Technology Research Project (No.222102320021).

Data Availability Statement: Data will be made available on request.

Conflicts of Interest: The authors declare no conflict of interest.

References

1. Deng, H.; Pepin, N.C.; Chen, Y.; Guo, B.; Zhang, S.; Zhang, Y.; Chen, X.; Gao, L.; Meibing, L.; Ying, C. Dynamics of Diurnal Precipitation Differences and Their Spatial Variations in China. *J. Appl. Meteorol. Climatol.* **2022**, *61*, 1015–1027. [CrossRef]
2. Wang, Y.; Li, C.; Liu, M.; Cui, Q.; Wang, H.; Lv, J.; Li, B.; Xiong, Z.; Hu, Y. Spatial characteristics and driving factors of urban flooding in Chinese megacities. *J. Hydrol.* **2022**, *613*, 128464. [CrossRef]
3. Wang, S.; Luo, P.; Xu, C.; Zhu, W.; Cao, Z.; Ly, S. Reconstruction of Historical Land Use and Urban Flood Simulation in Xi’an, Shannxi, China. *Remote Sens.* **2022**, *14*, 6067. [CrossRef]
4. Khajehei, S.; Ahmadalipour, A.; Shao, W.; Moradkhani, H. A Place-based Assessment of Flash Flood Hazard and Vulnerability in the Contiguous United States. *Sci. Rep.* **2020**, *10*, 448. [CrossRef] [PubMed]
5. Duan, W.; Zou, S.; Christidis, N.; Schaller, N.; Chen, Y.; Sahu, N.; Li, Z.; Fang, G.; Zhou, B. Changes in temporal inequality of precipitation extremes over China due to anthropogenic forcings. *npj Clim. Atmos. Sci.* **2022**, *5*, 33. [CrossRef]
6. Cao, Z.; Zhu, W.; Luo, P.; Wang, S.; Tang, Z.; Zhang, Y.; Guo, B. Spatially Non-Stationary Relationships between Changing Environment and Water Yield Services in Watersheds of China's Climate Transition Zones. *Remote Sens.* **2022**, *14*, 5078. [CrossRef]
7. Liu, J.; Shao, W.; Xiang, C.; Mei, C.; Li, Z. Uncertainties of urban flood modeling: Influence of parameters for different underlying surfaces. *Environ. Res.* **2020**, *182*, 108929. [CrossRef]
8. Luo, P.; Zheng, Y.; Wang, Y.; Zhang, S.; Yu, W.; Zhu, X.; Huo, A.; Wang, Z.; He, B.; Nover, D. Comparative Assessment of Sponge City Constructing in Public Awareness, Xi'an, China. *Sustainability* **2022**, *14*, 11653. [CrossRef]
9. Dong, S.; Yu, T.; Farahmand, H.; Mostafavi, A. Probabilistic modeling of cascading failure risk in interdependent channel and road networks in urban flooding. *Sustain. Cities Soc.* **2020**, *62*, 102398. [CrossRef]
10. Sohn, W.; Kim, J.-H.; Li, M.-H.; Brown, R. The influence of climate on the effectiveness of low impact development: A systematic review. *J. Environ. Manag.* **2019**, *236*, 365–379. [CrossRef]
11. Hossain, B. Role of organizations in preparedness and emergency response to flood disaster in Bangladesh. *Geoenviron. Disasters* **2020**, *7*, 33. [CrossRef]
12. Lumbroso, D.; Davison, M. Use of an agent-based model and Monte Carlo analysis to estimate the effectiveness of emergency management interventions to reduce loss of life during extreme floods. *J. Flood Risk Manag.* **2018**, *11*, S419–S433. [CrossRef]
13. Ahmadalipour, A.; Moradkhani, H. A data-driven analysis of flash flood hazard, fatalities, and damages over the CONUS during 1996–2017. *J. Hydrol.* **2019**, *578*, 124106. [CrossRef]
14. Luo, P.; Luo, M.; Li, F.; Qi, X.; Huo, A.; Wang, Z.; He, B.; Takara, K.; Nover, D.; Wang, Y. Urban flood numerical simulation: Research, methods and future perspectives. *Environ. Model. Softw.* **2022**, *156*, 105478. [CrossRef]
15. Lin, L.; Wei, X.; Luo, P.; Wang, S.; Kong, D.; Yang, J. Ecological Security Patterns at Different Spatial Scales on the Loess Plateau. *Remote Sens.* **2023**, *15*, 1011. [CrossRef]
16. Wang, X.; Luo, P.; Zheng, Y.; Duan, W.; Wang, S.; Zhu, W.; Zhang, Y.; Nover, D. Drought Disasters in China from 1991 to 2018: Analysis of Spatiotemporal Trends and Characteristics. *Remote Sens.* **2023**, *15*, 1708. [CrossRef]
17. Fang, J.; Hu, J.; Shi, X.; Zhao, L. Assessing disaster impacts and response using social media data in China: A case study of 2016 Wuhan rainstorm. *Int. J. Disaster Risk Reduct.* **2019**, *34*, 275–282. [CrossRef]
18. Zhu, W.; Cao, Z.; Luo, P.; Tang, Z.; Zhang, Y.; Hu, M.; He, B. Urban Flood-Related Remote Sensing: Research Trends, Gaps and Opportunities. *Remote Sens.* **2022**, *14*, 5505. [CrossRef]
19. Schumann, G.J.P.; Moller, D.K. Microwave remote sensing of flood inundation. *Phys. Chem. Earth Parts A/B/C* **2015**, *83–84*, 84–95. [CrossRef]
20. Songchon, C.; Wright, G.; Beevers, L. Quality assessment of crowdsourced social media data for urban flood management. *Comput. Environ. Urban Syst.* **2021**, *90*, 101690. [CrossRef]
21. Lin, A.; Wu, H.; Liang, G.; Cardenas-Tristan, A.; Wu, X.; Zhao, C.; Li, D. A big data-driven dynamic estimation model of relief supplies demand in urban flood disaster. *Int. J. Disaster Risk Reduct.* **2020**, *49*, 101682. [CrossRef]
22. Nkwunonwo, U.C.; Whitworth, M.; Baily, B. A review of the current status of flood modelling for urban flood risk management in the developing countries. *Sci. Afr.* **2020**, *7*, e00269. [CrossRef]
23. De Albuquerque, J.P.; Herfort, B.; Brenning, A.; Zipf, A. A geographic approach for combining social media and authoritative data towards identifying useful information for disaster management. *Int. J. Geogr. Inf. Sci.* **2015**, *29*, 667–689. [CrossRef]
24. Le Coz, J.; Patalano, A.; Collins, D.; Guillén, N.F.; García, C.M.; Smart, G.M.; Bind, J.; Chiaverini, A.; Le Boursicaud, R.; Dramais, G.; et al. Crowdsourced data for flood hydrology: Feedback from recent citizen science projects in Argentina, France and New Zealand. *J. Hydrol.* **2016**, *541*, 766–777. [CrossRef]
25. Tan, L.; Schultz, D.M. Damage classification and recovery analysis of the Chongqing, China, floods of August 2020 based on social-media data. *J. Clean. Prod.* **2021**, *313*, 127882. [CrossRef]
26. Wu, K.; Wu, J.; Ding, W.; Tang, R. Extracting disaster information based on Sina Weibo in China: A case study of the 2019 Typhoon Lekima. *Int. J. Disaster Risk Reduct.* **2021**, *60*, 102304. [CrossRef]
27. Guo, B.; Wu, H.; Pei, L.; Zhu, X.; Zhang, D.; Wang, Y.; Luo, P. Study on the spatiotemporal dynamic of ground-level ozone concentrations on multiple scales across China during the blue sky protection campaign. *Environ. Int.* **2022**, *170*, 107606. [CrossRef]
28. Fohringer, J.; Dransch, D.; Kreibich, H.; Schröter, K. Social media as an information source for rapid flood inundation mapping. *Nat. Hazards Earth Syst. Sci.* **2015**, *15*, 2725–2738. [CrossRef]

29. Rosser, J.F.; Leibovici, D.G.; Jackson, M.J. Rapid flood inundation mapping using social media, remote sensing and topographic data. *Nat. Hazards* **2017**, *87*, 103–120. [CrossRef]
30. Smith, L.; Liang, Q.; James, P.; Lin, W. Assessing the utility of social media as a data source for flood risk management using a real-time modelling framework. *J. Flood Risk Manag.* **2017**, *10*, 370–380. [CrossRef]
31. Li, Z.; Wang, C.; Emrich, C.T.; Guo, D. A novel approach to leveraging social media for rapid flood mapping: A case study of the 2015 South Carolina floods. *Cartogr. Geogr. Inf. Sci.* **2018**, *45*, 97–110. [CrossRef]
32. Zhang, Y.; Chen, Z.; Zheng, X.; Chen, N.; Wang, Y. Extracting the location of flooding events in urban systems and analyzing the semantic risk using social sensing data. *J. Hydrol.* **2021**, *603*, 127053. [CrossRef]
33. Feng, Y.; Sester, M. Extraction of Pluvial Flood Relevant Volunteered Geographic Information (VGI) by Deep Learning from User Generated Texts and Photos. *ISPRS Int. J. Geo-Inf.* **2018**, *7*, 39. [CrossRef]
34. Kankanamge, N.; Yigitcanlar, T.; Goonetilleke, A.; Kamruzzaman, M. Determining disaster severity through social media analysis: Testing the methodology with South East Queensland Flood tweets. *Int. J. Disaster Risk Reduct.* **2020**, *42*, 101360. [CrossRef]
35. Cheng, X.; Han, G.; Zhao, Y.; Li, L. Evaluating Social Media Response to Urban Flood Disaster: Case Study on an East Asian City (Wuhan, China). *Sustainability* **2019**, *11*, 5330. [CrossRef]
36. Wang, B.; Loo, B.P.Y.; Zhen, F.; Xi, G. Urban resilience from the lens of social media data: Responses to urban flooding in Nanjing, China. *Cities* **2020**, *106*, 102884. [CrossRef]
37. Liu, F.; Liu, X.; Xu, T.; Yang, G.; Zhao, Y. Driving Factors and Risk Assessment of Rainstorm Waterlogging in Urban Agglomeration Areas: A Case Study of the Guangdong-Hong Kong-Macao Greater Bay Area, China. *Water* **2021**, *13*, 770. [CrossRef]
38. Wang, Z.; Luo, P.; Zha, X.; Xu, C.; Kang, S.; Zhou, M.; Nover, D.; Wang, Y. Overview assessment of risk evaluation and treatment technologies for heavy metal pollution of water and soil. *J. Clean. Prod.* **2022**, *379*, 134043. [CrossRef]
39. Gudes, O.; Varhol, R.; Sun, Q.; Meuleners, L. Investigating articulated heavy-vehicle crashes in Western Australia using a spatial approach. *Accid. Anal. Prev.* **2017**, *106*, 243–253. [CrossRef]
40. Yoon, J.; Lee, S. Spatio-temporal patterns in pedestrian crashes and their determining factors: Application of a space-time cube analysis model. *Accid. Anal. Prev.* **2021**, *161*, 106291. [CrossRef]
41. Zhao, Y.; Ge, L.; Liu, J.; Liu, H.; Yu, L.; Wang, N.; Zhou, Y.; Ding, X. Analyzing hemorrhagic fever with renal syndrome in Hubei Province, China: A space–time cube-based approach. *J. Int. Med. Res.* **2019**, *47*, 3371–3388. [CrossRef] [PubMed]
42. Li, M.; Kwan, M.-P.; Yin, J.; Yu, D.; Wang, J. The potential effect of a 100-year pluvial flood event on metro accessibility and ridership: A case study of central Shanghai, China. *Appl. Geogr.* **2018**, *100*, 21–29. [CrossRef]
43. Yin, J.; Jing, Y.; Yu, D.; Ye, M.; Yang, Y.; Liao, B. A Vulnerability Assessment of Urban Emergency in Schools of Shanghai. *Sustainability* **2019**, *11*, 349. [CrossRef]
44. Yin, J.; Yu, D.; Lin, N.; Wilby, R.L. Evaluating the cascading impacts of sea level rise and coastal flooding on emergency response spatial accessibility in Lower Manhattan, New York City. *J. Hydrol.* **2017**, *555*, 648–658. [CrossRef]
45. Masuya, A.; Dewan, A.; Corner, R.J. Population evacuation: Evaluating spatial distribution of flood shelters and vulnerable residential units in Dhaka with geographic information systems. *Nat. Hazards* **2015**, *78*, 1859–1882. [CrossRef]
46. Shi, Y.; Wen, J.; Xi, J.; Xu, H.; Shan, X.; Yao, Q. A Study on Spatial Accessibility of the Urban Tourism Attraction Emergency Response under the Flood Disaster Scenario. *Complexity* **2020**, *2020*, 9031751. [CrossRef]
47. Shi, Y.; Yao, Q.; Wen, J.; Xi, J.; Li, H.; Wang, Q. A spatial accessibility assessment of urban tourist attractions emergency response in Shanghai. *Int. J. Disaster Risk Reduct.* **2022**, *74*, 102919. [CrossRef]
48. Yao, K.; Yang, S.; Tang, J. Rapid assessment of seismic intensity based on Sina Weibo—A case study of the changning earthquake in Sichuan Province, China. *Int. J. Disaster Risk Reduct.* **2021**, *58*, 102217. [CrossRef]
49. Wu, Z.; Zhang, Y.; Chen, Q.; Wang, H. Attitude of Chinese public towards municipal solid waste sorting policy: A text mining study. *Sci. Total Environ.* **2021**, *756*, 142674. [CrossRef]
50. Hou, G.; Chen, L. Regional commercial center identification based on POI big data in China. *Arab. J. Geosci.* **2021**, *14*, 1360. [CrossRef]
51. Zhang, L.; Xia, J. Flood Detection Using Multiple Chinese Satellite Datasets during 2020 China Summer Floods. *Remote Sens.* **2022**, *14*, 51. [CrossRef]
52. Dawei, W.; Hamzah, M.; Weng, N.G. Web crawler design, implementation and data analysis about Sina Weibo. In Proceedings of the 2019 3rd International Conference on Electronic Information Technology and Computer Engineering (EITCE), Xiamen, China, 18–20 October 2019; pp. 143–148. [CrossRef]
53. Gao, F.; Li, S.; Tan, Z.; Liao, S. Visualizing the Spatiotemporal Characteristics of Dockless Bike Sharing Usage in Shenzhen, China. *J. Geovis. Spat. Anal.* **2022**, *6*, 12. [CrossRef]
54. Huang, W.; DeVries, B.; Huang, C.; Lang, M.W.; Jones, J.W.; Creed, I.F.; Carroll, M.L. Automated Extraction of Surface Water Extent from Sentinel-1 Data. *Remote Sens.* **2018**, *10*, 797. [CrossRef]
55. Jia, S.; Xue, D.; Li, C.; Zheng, J.; Li, W. Study on new method for water area information extraction based on Sentinel—1 data. *Yangtze River* **2019**, *50*, 213–217.
56. Tian, P.; Liu, Y.; Li, J.; Pu, R.; Cao, L.; Zhang, H.; Ai, S.; Yang, Y. Mapping Coastal Aquaculture Ponds of China Using Sentinel SAR Images in 2020 and Google Earth Engine. *Remote Sens.* **2022**, *14*, 5372. [CrossRef]
57. Huang, Q.; Cervone, G.; Zhang, G. A cloud-enabled automatic disaster analysis system of multi-sourced data streams: An example synthesizing social media, remote sensing and Wikipedia data. *Comput. Environ. Urban Syst.* **2017**, *66*, 23–37. [CrossRef]

58. Yang, T.; Xie, J.; Li, G.; Zhang, L.; Mou, N.; Wang, H.; Zhang, X.; Wang, X. Extracting Disaster-Related Location Information through Social Media to Assist Remote Sensing for Disaster Analysis: The Case of the Flood Disaster in the Yangtze River Basin in China in 2020. *Remote Sens.* **2022**, *14*, 1199. [CrossRef]
59. Zhang, Q.; Wu, Z.; Zhang, H.; Dalla Fontana, G.; Tarolli, P. Identifying dominant factors of waterlogging events in metropolitan coastal cities: The case study of Guangzhou, China. *J. Environ. Manag.* **2020**, *271*, 110951. [CrossRef]
60. Kim, J.; Hastak, M. Social network analysis: Characteristics of online social networks after a disaster. *Int. J. Inf. Manag.* **2018**, *38*, 86–96. [CrossRef]
61. Karunarathne, A.Y.; Lee, G. The geographies of the dynamic evolution of social networks for the flood disaster response and recovery. *Appl. Geogr.* **2020**, *125*, 102274. [CrossRef]